Local Structure and Surface Properties of Co$_x$Zn$_{1-x}$O Thin Films for Ozone Gas Sensing

Ariadne C. Catto,*,[†] Luís F. da Silva,*,[‡] Maria Inês B. Bernardi,[†] Sandrine Bernardini,[§] Khalifa Aguir,[§] Elson Longo,[‡] and Valmor R. Mastelaro[†]

[†]Institute of Physics of São Carlos, University of São Paulo, Av. Trabalhador Sãocarlense 400, 13566-590, São Carlos, SP Brazil
[‡]Institute of Chemistry, São Paulo State University, P.O. Box 355, 14800-900 Araraquara, SP Brazil
[§]Aix-Marseille University, CNRS, IM2NP 7334, Av. E. N. Neimen, 13397 Marseille, France

Ⓢ Supporting Information

ABSTRACT: A detailed study of the structural, surface, and gas-sensing properties of nanostructured Co$_x$Zn$_{1-x}$O films is presented. X-ray diffraction (XRD) analysis revealed a decrease in the crystallization degree with increasing Co content. The X-ray absorption near-edge structure (XANES) and X-ray photoelectron spectroscopies (XPS) revealed that the Co^{2+} ions preferentially occupied the Zn^{2+} sites and that the oxygen vacancy concentration increased as the amount of cobalt increased. Electrical measurements showed that the Co dopants not only enhanced the sensor response at low ozone levels (ca. 42 ppb) but also led to a decrease in the operating temperature and improved selectivity. The enhancement in the gas-sensing properties was attributed to the presence of oxygen vacancies, which facilitated ozone adsorption.

KEYWORDS: zinc oxide, cobalt, XANES spectroscopy, XPS, gas sensor, ozone
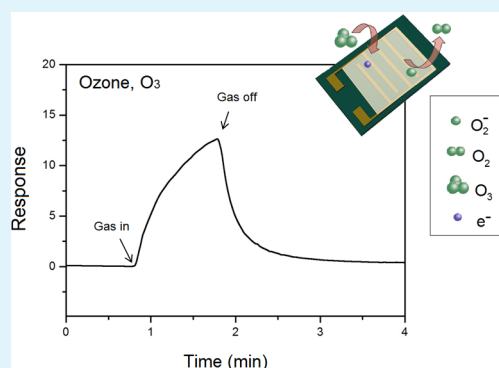
1. INTRODUCTION

The environmental monitoring of atmospheric gas pollutants such as NO$_2$, NO$_x$, O$_3$, CO, and NH$_3$ in urban areas has received attention from international organizations due to their adverse effects on human health.[1−3] Most of these pollutants are mainly produced by industrial and agricultural activities, automobiles, and even domestic activities. In contrast, ozone is not emitted directly into the atmosphere; it is produced by photochemical reactions between nitrogen oxides (NO$_x$), carbon monoxide (CO), and volatile organic compounds (VOCs) in the presence of sunlight.[4] Ozone (O$_3$) is a powerful oxidizing reagent and very strong disinfectant; however, even in low concentrations, ground-level ozone might negatively impact human health.[3] According to the World Health Organization (WHO), relatively high ozone concentrations in the air can cause breathing problems, trigger asthma, reduce lung function, and cause lung diseases.[5]

Pure and/or doped zinc oxide (ZnO) has been widely studied as a chemiresistor due to its chemical sensitivity to different harmful gases.[2,6,7] The main advantage of these materials is their high surface-to-volume ratio, which enhances their gas-sensing performance.[8] Despite the progress in developing sensor devices based on ZnO sensing materials, their sensitivity and selectivity must still be improved. Recently, researchers have focused on developing efficient semiconductor composites, such as p-Co$_3$O$_4$/n-ZnO for gas-sensing applications.[9] Cobalt and zinc have been widely employed as gas-sensing materials due to their ability to activate molecular gases

(oxygen, liquefied petroleum gas, carbon dioxide, etc.),[10] chemical sensitivity, high chemical stability, and nontoxicity.[2] Another efficient way to enhance the gas-sensing properties of ZnO is to dope transition metals (e.g., Co, Fe, and Ni) into the ZnO network.[11−13] Co$_x$Zn$_{1-x}$O solid solutions have attracted attention because the ZnO physical and chemical properties can be altered by Co doping.[14−16] Introducing Co into the ZnO structure as a substitutional atom can modify the local structure, resulting in an increase in the oxygen vacancy concentration,[17] which effectively tunes the sensing properties. Although several papers have reported the influence of Co ions on the gas-sensing performance of ZnO, the ozone gas-sensing properties of Co$_x$Zn$_{1-x}$O solid solutions have been rarely studied. Furthermore, their sensing response, selectivity, and long-term stability must be improved to meet the requirements of real-time toxic gas monitoring.

Herein, a detailed investigation of the effects of Co ions on the long- and short-range structures and the surface and ozone gas-sensing properties of nanostructured ZnO films is presented. The properties of Co$_x$Zn$_{1-x}$O were studied by X-ray diffraction (XRD), X-ray absorption near-edge structure spectroscopy (XANES), X-ray photoelectron spectroscopy (XPS), and atomic force microscopy (AFM). Gas-sensing measurements revealed that the ozone gas-sensing properties

were improved by increasing the Co content. Compared to pristine ZnO, Co-doped ZnO films had a higher ozone sensor response, good selectivity, and lower operating temperature.

2. EXPERIMENTAL SECTION

2.1. Thin-Film Preparation. $Co_xZn_{1-x}O$ thin films with $x = 0.0$, 0.025, and 0.05 mol % of cobalt were prepared via the polymeric precursor method. This synthesis route has been used extensively to prepare polycation oxides. The advantages of this method are good composition control, reproducibility, and, in particular, particle size control in the range from nanometers to micrometers.[18−20] Zinc(II) nitrate hexahydrate ($Zn(NO_3)_2 \cdot 6H_2O$, Aldrich, ≥99%) and cobalt(II) nitrate hexahydrate ($Co(NO_3)_2 \cdot 6H_2O$, Aldrich, ≥98%) precursors were separately dissolved in 50 mL of deionized water to obtain 0.04 M solutions. Appropriate amounts of these solutions were then mixed to obtain a final solution with a Zn/Co molar ratio of 1. Finally, 20 mg of citric acid ($C_6H_8O_7$, Synth, 99.5%) was added to this solution under constant stirring at 100 °C. After the citric acid was dissolved, the temperature was increased to 150 °C, and 13 mL of ethylene glycol ($C_2H_6O_2$, Synth, 99.5%) was then added to the precursor solution to obtain a polymeric resin. Finally, the resin viscosity was adjusted to 12 cP using a rheometer (Brookfield, LVDV-III Ultra). The solution was spin-coated onto different substrates at 10 000 rpm for 60 s, and water was subsequently evaporated from the sample using a hot plate at 100 °C for 30 min to obtain the $Co_xZn_{1-x}O$ thin films. The substrates included borosilicate glass, c-Si (100), and SiO_2/Si with 120 nm thick Pt electrodes (illustrated in Figure 1). A two-stage annealing treatment
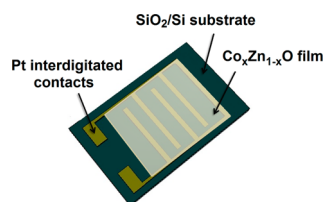
**Figure 1.** Schematic illustration of the gas sensor device structure.

was then applied. The samples were initially heated to 300 °C for 30 min in air at a rate of 1 °C min^{-1} to pyrolyze the organic compounds and then annealed to 500 °C for 2 h at a rate of 5 °C min^{-1} for crystallization.

2.2. Characterization Techniques. The samples were characterized by X-ray diffraction with a Cu Kα radiation source (Rigaku, Ultima IV) at room temperature. Typical $\theta-2\theta$ scans were performed in the range of 25−80° with a step size of 0.02° and scanning rate of 2° min^{-1}. The surface morphologies were investigated using an atomic force microscope (FlexAFM 3, Nanosurf, Switzerland) in tapping mode. For all the measurements, Tap150Al-G cantilevers were employed with a force constant of 5 N m^{-1}. The AFM data were analyzed using the free Gwyddion 2.45 software. The X-ray absorption near-edge structure (XANES) measurements were performed at beamline XAFS2 at the Brazilian Synchrotron Light Laboratory (LNLS). The Co K-edge XANES spectra were collected using a 15-element Ge solid-state detector (Ge-15) in fluorescence mode at room temperature in the range of 7700−7780 eV with an energy step size of 0.3 eV. For comparison, the background was removed from the spectra, which were then normalized by the first extended X-ray absorption fine structure (EXAFS) oscillation using MAX software.[21] X-ray photoelectron spectroscopy (XPS) analyses were performed on a Thermo Scientific K-Alpha spectrometer using monochromatic Al Kα (1486.6 eV) radiation. Peak decomposition was performed using a 70% Gaussian and 30% Lorentzian line shape with a Shirley nonlinear sigmoid-type baseline. The binding energies were corrected for charging effects by assigning a value of 284.8 eV to the adventitious C 1s line. The data were analyzed using CasaXPS software (Casa Software Ltd., U.K.).

2.3. Gas-Sensing Measurements. The sample on the SiO_2/Si substrate with 120 nm thick Pt electrodes was inserted into a chamber to control the temperature at different ozone concentrations. Ozone gas was formed by oxidizing oxygen molecules in dry air (500 SCCM) under a calibrated pen-ray UV lamp (UVP, model P/N 90-0004-01) that provided ozone in a concentration range of 42−560 ppb. The ozone levels were calibrated by a toxic gas detector (ATI, model F12). The ozone-containing dry air was blown directly onto the sample, which was placed in a heated holder system. To determine the selectivity, NO_2 and CO gas-sensing measurements were performed, for concentration from 1 to 5 ppm. The applied dc voltage was 1 V, and the electrical resistance was measured by an electrometer (Keithley, 6514). The sensor response (S) was defined as $S = (R_{ozone} - R_{air})/R_{air} = \Delta R/R$, where R_{ozone} and R_{air} are the electrical resistances of the sensor upon exposure to ozone gas and dry air, respectively. The sensor response time was defined as the time required for the electrical resistance to reach 90% of the initial value when exposed to ozone gas. Likewise, the recovery time was defined as the time required for the electrical resistance to recover 90% of the initial value after the ozone gas flow was switched off.

3. RESULTS AND DISCUSSION

Figure 2 shows the XRD patterns of $Co_xZn_{1-x}O$ samples annealed at 500 °C. All the diffraction peaks were indexed to
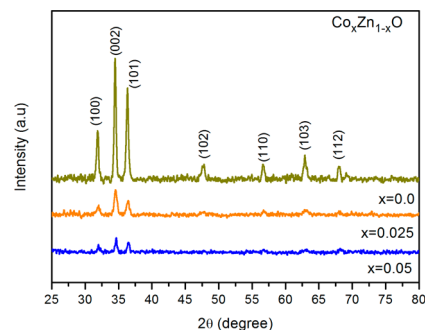
Figure 2. X-ray diffraction patterns of the $Co_xZn_{1-x}O$ thin films.

the ZnO hexagonal wurtzite structure with $P6_3mc$ symmetry (Joint Committee on Powder Diffraction Standard (JCPDS) file 36-1451). No other secondary phases such as cobalt oxides, were observed in the XRD patterns within the detection limit of the measurements. However, the XRD peak intensities decreased significantly as the amount of Co increased. A similar result was reported for ZnO:Co thin films prepared by the sol−gel method[22] and was attributed to crystal defects caused by the difference in the Zn and Co ionic radii (0.72 Å for Co^{2+} and 0.74 Å for Zn^{2+}).[22,23] This difference in the ionic radii also led to a decrease in the lattice parameter; hence, the XRD peaks were slightly shifted to higher 2θ angles. Both of these results indicate that Co atoms replaced Zn atoms in the ZnO lattice.[24−26]

Figure 3 shows the Co K-edge XANES spectra of cobalt-based reference compounds (CoO, $CoAl_2O_4$, and Co_3O_4) and the $Co_xZn_{1-x}O$ samples. The XANES pre-edge and edge features provide qualitative information on the local symmetry and oxidation states, respectively, of the cobalt atoms.[24] The intensity of the pre-edge feature A, which is due to electron transitions from the occupied 1s to unoccupied 3d states, is related to the local symmetry around the Co atoms; a tetrahedral cobalt compound exhibits a higher intensity than an octahedral compound. The edge energy B indicates the oxidation state of the absorber atom.[24,27,28] Accordingly, as shown in Figure 3b, the tetrahedral reference compound
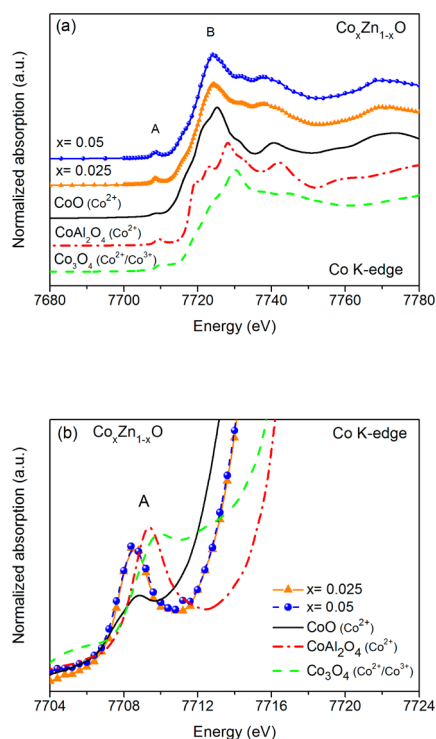
Figure 3. Co K-edge XANES spectra of the $Co_xZn_{1-x}O$ thin films and cobalt oxide reference compounds (CoO, $CoAl_2O_4$, and Co_3O_4). (a) Full spectra and (b) the pre-edge region.

$(CoAl_2O_4)$ has a higher peak A intensity than the octahedral reference compound (CoO). Therefore, the high peak A intensities in the XANES spectra of the $Co_xZn_{1-x}O$ thin films indicate that the majority of the doped Co ions occupied tetrahedral sites.[24,29] The K-edge energies of the $Co_xZn_{1-x}O$ thin films were similar to each other and to those of the Co^{2+} reference compounds, indicating that the oxidation state of most of the Co ions was +2. Thus, the XANES results show that the Co ions preferentially substituted for Zn atoms in the ZnO crystal lattice.

Figure 4a shows the XPS survey spectra of the $Co_xZn_{1-x}O$ samples. The peaks in these spectra were indexed and revealed the presence of Zn, Co, and O; only carbon was detect as an impurity because the samples were exposed to the atmosphere before the measurements.[30]

In the high-resolution Zn $2p_{3/2}$ XPS spectra shown in Figure 4b, a peak was observed at 1021.35 eV, which is in good agreement with previous studies. A comparison of the high-resolution Zn $2p_{3/2}$ XPS spectra of the samples shows that the peak was slightly shifted after cobalt was doped into ZnO. Figure 4c shows the high-resolution Co 2p XPS spectra, in which the Co $2p_{3/2}$ and Co $2p_{1/2}$ peaks were located at 780.7 and 796.4 eV, respectively.[25]

The binding energies of these peaks were not dependent on the Co concentration, suggesting that the local electronic structure of Co was not affected by the Co concentration. The energy difference between the Co $2p_{3/2}$ and Co $2p_{1/2}$ peaks (spin−orbit splitting) was approximately 15.65 eV, which is close to the standard value for CoO (15.5 eV) and consistent with the Co divalent state ($3d^7$; $S = 3/2$).[30−34] A shakeup satellite structure was observed on the lower binding energy side of both peaks for both samples, and the satellite peak at
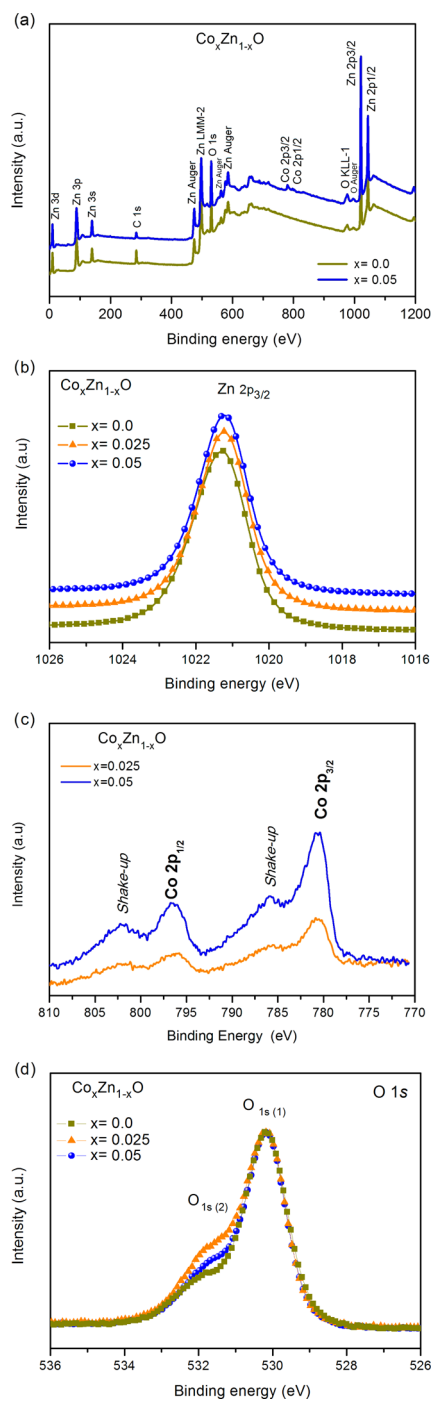
**Figure 4.** XPS spectra of the $Co_xZn_{1-x}O$ samples. (a) Survey scan, (b) Zn 2p, (c) Co 2p, and (d) O 1s.

785.4 eV was approximately 5 eV higher in energy than the Co $2p_{3/2}$ main peak, which is characteristic of the Co^{2+} ion.[31,32]

The high-resolution O 1s spectra were also measured and deconvoluted into two Gaussian−Lorentzian components as illustrated in Figure 4d. The analysis revealed the presence of two oxygen species, labeled as $O_{1s(1)}$ and $O_{1s(2)}$. The lower-energy peak at 530.1 eV ($O_{1s(1)}$) was attributed to the oxygen anions (O^{2-}) bound to the metal cations (Zn^{2+} or substitutional Co^{2+}) in the tetrahedral sites of the hexagonal wurtzite structure. The second component at approximately 531.2 eV ($O_{1s(2)}$) was assigned to weakly bound −OH species and carbonate species at the sample surface.[30,31,35,36] Variations in

the $O_{1s(2)}$ component were attributed to differences in the oxygen vacancies or defects at the sample surface or oxygen-deficient regions within the ZnO matrix.[35,37] Variation in the oxygen vacancy or defect concentration in the films might facilitate the chemisorption process.[38] The deconvoluted O 1s XPS spectra of the $Co_xZn_{1-x}O$ samples are shown in Figure S1.

Figure 5 shows the AFM images of the $Co_xZn_{1-x}O$ samples. All the samples exhibited a typical nanocrystalline film surface
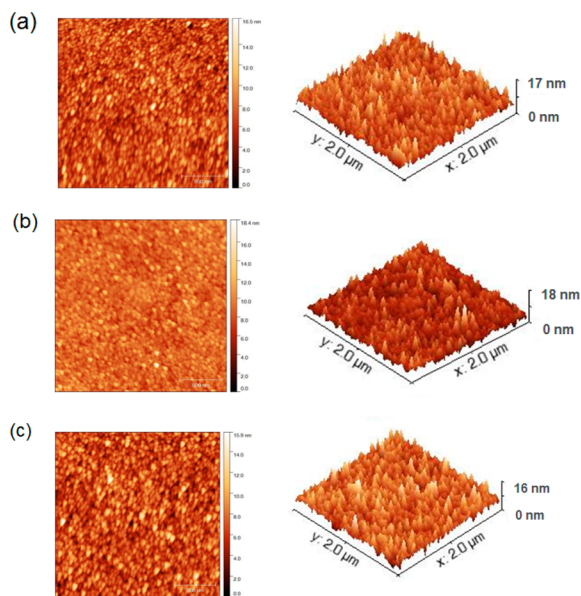
Figure 5. AFM images of the $Co_xZn_{1-x}O$ samples. (a) $x = 0.0$, (b) $x = 0.025$, and (c) $x = 0.05$.

morphology, and the average grain sizes were 34 ($x = 0.0$), 29 ($x = 0.025$), and 28 nm ($x = 0.05$). Furthermore, the root-mean-square roughness values (R_{rms}) of the $Co_xZn_{1-x}O$ samples ranged from 1.2 to 1.8 nm, indicating that they were not significantly affected.

The effects of the Co content on the ozone gas-sensing properties of the ZnO samples were evaluated. First, the $Co_xZn_{1-x}O$ samples were exposed to 84 ppb of ozone at different operating temperatures (T_{opt}). The results in Figure 6 show that the maximum response temperature decreased from 250 °C for $x = 0.0$ to 200 °C for $x = 0.05$. These findings indicate that Co doping enhanced the ZnO sensor response and provided additional sites for ozone adsorption. The relationships between the sensor response and operating temperature for the $Co_xZn_{1-x}O$ samples are presented in
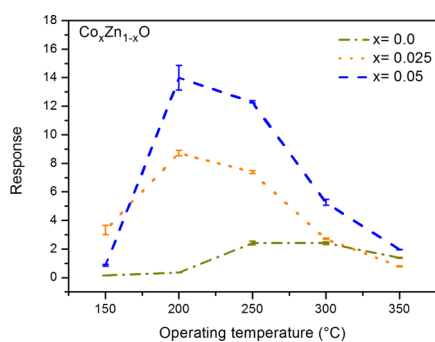
Figure 6. Gas sensor response of the $Co_xZn_{1-x}O$ samples when exposed to 84 ppb of O_3 as a function of the operating temperature.

Figure 6. This figure shows that the sample response initially increased with increasing operating temperature, reached a maximum value, and then decreased as the temperature was further increased. This behavior can be explained as follows: at lower temperatures, chemical activation of the analyte by the sensing material was low, resulting in a lower gas-sensing performance. On the other hand, at higher operating temperatures, the adsorbed gas molecules could desorb before reacting due to their enhanced activation, leading to a decreased sensor response. Thus, the optimal operating temperature was determined by the equilibrium between the surface reactions, i.e., the adsorption and desorption processes.[38]

The $Co_xZn_{1-x}O$ samples were then exposed to different ozone concentrations (42 to 560 ppb) at 200 °C, and their responses are shown in Figure 7. Three 60 s cycles were
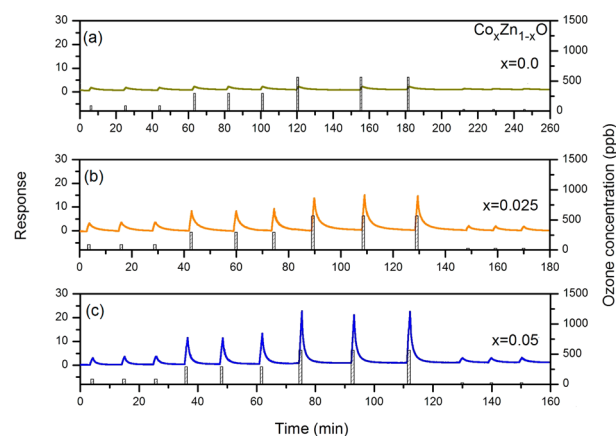
Figure 7. Gas-sensing response of the $Co_xZn_{1-x}O$ thin films exposed to different ozone levels (42, 84, 290, and 560 ppb) at 200 °C. (a) $x = 0.0$, (b) $x = 0.025$, and (c) $x = 0.05$.

performed at each concentration. The response of the $Co_xZn_{1-x}O$ materials upon exposure to ozone (O_3) gas can be explained by the following reactions.[2] First, when the $Co_xZn_{1-x}O$ samples were exposed to air, oxygen molecules adsorbed on the semiconductor surface.

$$O_{2(g)} \rightarrow O_{2(ads)} \tag{1}$$

The oxygen molecules captured free electrons from the $Co_xZn_{1-x}O$ conduction band, forming oxygen anions.[2,39] At an operating temperature of 200 °C, the ionic O^- species was dominant.[2,39]

$$O_{2(ads)} + 2e^- \rightarrow 2O^-_{(ads)} \tag{2}$$

Upon exposure to O_3 gas, O_3 molecules adsorbed and reacted on the $Co_xZn_{1-x}O$ surfaces, as shown in the following reactions

$$O_{3(g)} + e^- \rightarrow O_3^-{}_{(ads)} \tag{3}$$

$$O_3^-{}_{(ads)} + O^-_{(ads)} + 2e^- \rightarrow O_{2(g)} + 2O_2^-{}_{(ads)} \tag{4}$$
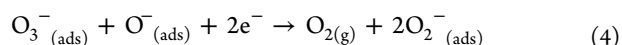
These reactions led to a wider depletion layer at the $Co_xZn_{1-x}O$ surface, hindering charge carrier flux and resulting in an increase in the electrical resistance when the sensing material was exposed to the oxidizing gas.[6]

Figure 7 shows that all the cycles were reversible, indicating that the samples exhibited stable, reproducible responses. In addition, after several exposure cycles, the $Co_xZn_{1-x}O$ samples

could still detect low ozone concentrations, demonstrating good reversibility. Furthermore, response saturation was not observed, even at the highest ozone concentration evaluated. The sensor response was significantly enhanced by Co doping in the concentration range studied. $Co_{0.05}Zn_{0.95}O$ exhibited a higher response (ca. 5 times) than pristine ZnO at 42 ppb. The response time was similar for all the samples (~40 s), but the recovery time decreased from 8.5 to 6 min with increasing Co content (see Table S1). This behavior can be attributed to the catalytic role of the doped Co in the samples, which improved the desorption kinetics.[40]

The enhanced sensor response of the Co-doped ZnO samples to ozone gas might be due to the effects of the Co ions on the ZnO electronic and surface properties and the large oxygen vacancy concentration and not to changes in the surface morphology because it was unaltered by the Co doping. Similar observations were reported by Zhu and co-workers for Co-doped ZnO microsphere gas sensors for 1,2-dichloroethane. These authors observed that although the cobalt ions did not affect the morphology the gas sensor response was improved due to the active sites provided by the metal doping.[41] Doping improves the gas-sensing performance by optimizing the sample morphology, increasing the surface-to-volume ratio and leading to the formation of additional active sites.[42,43] Theoretical studies have elucidated the role of oxygen vacancies in enhancing the gas-sensing ability of ZnO nanostructures.[44,45] An and co-workers[45] used density functional theory to investigate the reactions between different gases and ZnO nanotube surfaces with and without oxygen vacancies. They found that defects (e.g., oxygen vacancies) strengthened the bonding interactions between the analyte molecules and ZnO nanotubes and generated additional gas molecule adsorption sites compared to the defect-free surface.

Gas selectivity and long-term stability are the most important sensor parameters in practical applications. Figure 8 shows the
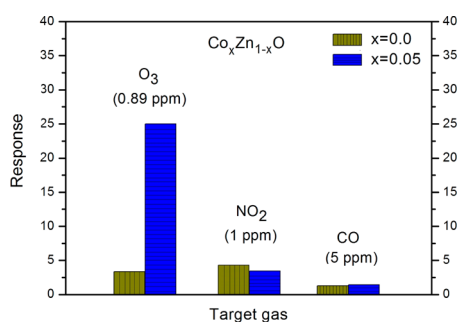
Figure 8. Comparison of the responses of the $Co_xZn_{1-x}O$ thin films to different gases.

sensor response (S) values of the $Co_xZn_{1-x}O$ thin films when exposed to oxidizing (O_3 and NO_2) and reducing (CO) gases at 200 °C. To compare the sensor responses to the different gases, 0.89 ppm of O_3, 1.0 ppm of NO_2, and 5.0 ppm of CO were used. The Co-doped ZnO film exhibited a higher response to ozone than ZnO and a higher response to O_3 ($S = 25.0$) than to NO_2 ($S = 3.5$) and CO ($S = 1.4$). In contrast, ZnO exhibited comparable responses to all the gases studied.

The long-term stability was also evaluated by exposing the sensor to 290 ppb of O_3 for a 9-month period, and the results are shown in Figure 9. The gas sensor response varied slightly, demonstrating the potential of the nanostructured $Co_xZn_{1-x}O$ materials for detecting gases at low concentrations over long
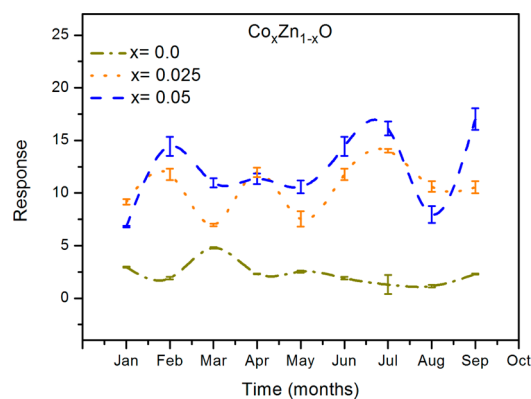
Figure 9. Gas sensor response of the $Co_xZn_{1-x}O$ thin films during exposure to 290 ppb of ozone for 9 months.

time periods. Based on these results, Co-doped ZnO thin films are promising sensing materials for ozone sensors.

4. CONCLUSIONS

This paper reports a versatile approach for preparing nanostructured $Co_xZn_{1-x}O$ films for use as promising ozone gas sensors. XRD and XPS analyses revealed that Co doping decreased the thin film crystallinity and increased the oxygen vacancy concentration. Additionally, XANES spectroscopy showed that the Co^{2+} ions preferentially occupied the Zn^{2+} sites in $Co_xZn_{1-x}O$. The gas-sensing experiments revealed that the ozone-sensing performance increased considerably with increasing Co content. Compared to pristine ZnO, Co-doped ZnO not only had a lower working temperature but also exhibited a higher sensor response and good selectivity to ozone. The enhanced sensor properties were due to the catalytic activity of the doped Co ions and the presence of oxygen vacancies at the semiconductor surface, which facilitated ozone chemisorptions. This chemical method provides a facile, efficient route to manufacturing ozone gas sensor devices with remarkable properties.

■ ASSOCIATED CONTENT

ⓢ Supporting Information

The Supporting Information is available free of charge on the ACS Publications website at DOI: 10.1021/acsami.6b08589.

> Details of the XPS O 1s deconvolution procedure and the gas-sensing properties (response and recovery times) of the $Co_xZn_{1-x}O$ samples (PDF)

■ AUTHOR INFORMATION

Corresponding Authors
*E-mail: ade.catto@gmail.com.
*E-mail: lfsilva83@gmail.com.

Author Contributions

All authors have given approval to the final version of the manuscript.

Notes

The authors declare no competing financial interest.

■ ACKNOWLEDGMENTS

■ REFERENCES

(1) Maeng, S.; Kim, S.-W.; Lee, D.-H.; Moon, S.-E.; Kim, K.-C.; Maiti, A. SnO_2 Nanoslab as NO_2 Sensor: Identification of the NO_2 Sensing Mechanism on a SnO_2 Surface. *ACS Appl. Mater. Interfaces* **2014**, *6* (1), 357−363.

(2) Barreca, D.; Bekermann, D.; Comini, E.; Devi, A.; Fischer, R. A.; Gasparotto, A.; Maccato, C.; Sada, C.; Sberveglieri, G.; Tondello, E. Urchin-like ZnO Nanorod Arrays for Gas Sensing Applications. *CrystEngComm* **2010**, *12* (11), 3419−3421.

(3) Korotcenkov, G.; Cho, B. K. Ozone Measuring: What Can Limit Application of SnO_2-Based Conductometric Gas Sensors? *Sens. Actuators, B* **2012**, *161* (1), 28−44.

(4) von Schneidemesser, E.; Monks, P. S.; Allan, J. D.; Bruhwiler, L.; Forster, P.; Fowler, D.; Lauer, A.; Morgan, W. T.; Paasonen, P.; Righi, M.; Sindelarova, K.; Sutton, M. A. Chemistry and the Linkages between Air Quality and Climate Change. *Chem. Rev.* **2015**, *115* (10), 3856−3897.

(5) da Silva, L. F.; Catto, A. C.; Avansi, W.; Cavalcante, L. S.; Andres, J.; Aguir, K.; Mastelaro, V. R.; Longo, E. A Novel Ozone Gas Sensor Based on One-Dimensional (1D) a-Ag_2WO_4 Nanostructures. *Nanoscale* **2014**, *6* (8), 4058−4062.

(6) Catto, A. C.; da Silva, L. F.; Ribeiro, C.; Bernardini, S.; Aguir, K.; Longo, E.; Mastelaro, V. R. An Easy Method of Preparing Ozone Gas Sensors Based on ZnO Nanorods. *RSC Adv.* **2015**, *5* (25), 19528−19533.

(7) Rai, P.; Kim, Y.-S.; Song, H.-M.; Song, M.-K.; Yu, Y.-T. The Role of Gold Catalyst on the Sensing Behavior of ZnO Nanorods for CO and NO_2 Gases. *Sens. Actuators, B* **2012**, *165* (1), 133−142.

(8) da Silva, L. F.; Mastelaro, V. R.; Catto, A. C.; Escanhoela, C. A.; Bernardini, S.; Zílio, S. C.; Longo, E.; Aguir, K. Ozone and Nitrogen Dioxide Gas Sensor Based on a Nanostructured $SrTi_{0.85}Fe_{0.15}O_3$ Thin Film. *J. Alloys Compd.* **2015**, *638*, 374−379.

(9) Bekermann, D.; Gasparotto, A.; Barreca, D.; Maccato, C.; Comini, E.; Sada, C.; Sberveglieri, G.; Devi, A.; Fischer, R. A. Co_3O_4/ZnO Nanocomposites: From Plasma Synthesis to Gas Sensing Applications. *ACS Appl. Mater. Interfaces* **2012**, *4* (2), 928−934.

(10) Gawande, K. B.; Gawande, S. B.; Thakare, S. R.; Mate, V. R.; Kadam, S. R.; Kale, B. B.; Kulkarni, M. V. Effect of Zinc: Cobalt Composition in $ZnCo_2O_4$ Spinels for Highly Selective Liquefied Petroleum Gas Sensing at Low and High Temperatures. *RSC Adv.* **2015**, *5* (50), 40429−40436.

(11) Rambu, A. P.; Ursu, L.; Iftimie, N.; Nica, V.; Dobromir, M.; Iacomi, F. Study on Ni-doped ZnO Films as Gas Sensors. *Appl. Surf. Sci.* **2013**, *280*, 598−604.

(12) Zhang, W.-H.; Zhang, W.-D.; Zhou, J.-F. Solvent Thermal Synthesis and Gas-Sensing Properties of Fe-doped ZnO. *J. Mater. Sci.* **2010**, *45* (1), 209−215.

(13) Li, Y.-J.; Li, K.-M.; Wang, C.-Y.; Kuo, C.-I.; Chen, L.-J. Low-Temperature Electrodeposited Co-doped ZnO Nanorods with Enhanced Ethanol and CO Sensing Properties. *Sens. Actuators, B* **2012**, *161* (1), 734−739.

(14) Bilecka, I.; Luo, L.; Djerdj, I.; Rossell, M. D.; Jagodič, M.; Jagličić, Z.; Masubuchi, Y.; Kikkawa, S.; Niederberger, M. Microwave-Assisted Nonaqueous Sol−Gel Chemistry for Highly Concentrated ZnO-Based Magnetic Semiconductor Nanocrystals. *J. Phys. Chem. C* **2011**, *115* (5), 1484−1495.

(15) Quan, Z.; Zhang, X.; Liu, W.; Li, X.; Addison, K.; Gehring, G. A.; Xu, X. Enhanced Room Temperature Magnetoresistance and Spin Injection from Metallic Cobalt in Co/ZnO and Co/ZnAlO Films. *ACS Appl. Mater. Interfaces* **2013**, *5* (9), 3607−3613.

(16) Hodges, J. M.; Fenton, J. L.; Gray, J. L.; Schaak, R. E. Colloidal ZnO and $Zn_{1-x}Co_xO$ Tetrapod Nanocrystals with Tunable Arm Lengths. *Nanoscale* **2015**, *7* (40), 16671−16676.

(17) Mesquita, A.; Rhodes, F. P.; da Silva, R. T.; Neves, P. P.; de Zevallos, A. O.; Andreeta, M. R. B.; de Lima, M. M., Jr.; Cantarero, A.; da Silva, I. S.; Boselli, M. A.; Gratens, X.; Chitta, V. A.; Doriguetto, A. C.; Ferraz, W. B.; Sabioni, A. C. S.; de Carvalho, H. B. Dynamics of the Incorporation of Co into the Wurtzite ZnO Matrix and Its Magnetic Properties. *J. Alloys Compd.* **2015**, *637*, 407−417.

(18) da Silva, L. F.; M'Peko, J.-C.; Andrés, J.; Beltrán, A.; Gracia, L.; Bernardi, M. I. B.; Mesquita, A.; Antonelli, E.; Moreira, M. L.; Mastelaro, V. R. Insight into the Effects of Fe Addition on the Local Structure and Electronic Properties of $SrTiO_3$. *J. Phys. Chem. C* **2014**, *118* (9), 4930−4940.

(19) Pontes, D. S. L.; Pontes, F. M.; da Silva, L. F.; Chiquito, A. J.; Pizani, P. S.; Longo, E. Influence of a Co-Substituted A-Site on Structural Characteristics and Ferroelectricity of (Pb, Ba, Ca)TiO_3 Complex Perovskites: Analysis of Local-, Medium- and Long-Range Order. *J. Sol-Gel Sci. Technol.* **2014**, *69* (3), 605−616.

(20) Arima, M.; Kakihana, M.; Nakamura, Y.; Yashima, M.; Yoshimura, M. Polymerized Complex Route to Barium Titanate Powders Using Barium-Titanium Mixed-Metal Citric Acid Complex. *J. Am. Ceram. Soc.* **1996**, *79* (11), 2847−2856.

(21) Alain, M.; Jacques, M.; Diane, M.-B.; Karine, P. MAX: Multiplatform Applications for XAFS. *J. Phys. Conf. Ser.* **2009**, *190* (1), 12034.

(22) Caglar, Y. Sol−gel Derived Nanostructure Undoped and Cobalt Doped ZnO: Structural, Optical and Electrical Studies. *J. Alloys Compd.* **2013**, *560* (0), 181−188.

(23) Arshad, M.; Azam, A.; Ahmed, A. S.; Mollah, S.; Naqvi, A. H. Effect of Co Substitution on the Structural and Optical Properties of ZnO Nanoparticles Synthesized by Sol−gel Route. *J. Alloys Compd.* **2011**, *509* (33), 8378−8381.

(24) He, R.; Hocking, R. K.; Tsuzuki, T. Co-Doped ZnO Nanopowders: Location of Cobalt and Reduction in Photocatalytic Activity. *Mater. Chem. Phys.* **2012**, *132* (2−3), 1035−1040.

(25) Fassbender, J.; McCord, J. Control of Saturation Magnetization, Anisotropy, and Damping due to Ni Implantation in Thin $Ni_{81}Fe_{19}$ Layers. *Appl. Phys. Lett.* **2006**, *88* (25), 252501.

(26) Shatnawi, M.; Alsmadi, A. M.; Bsoul, I.; Salameh, B.; Alna'washi, G. A.; Al-Dweri, F.; El Akkad, F. Magnetic and Optical Properties of Co-Doped ZnO Nanocrystalline Particles. *J. Alloys Compd.* **2016**, *655*, 244−252.

(27) Jiang, T.; Ellis, D. E. X-Ray Absorption near Edge Structures in Cobalt Oxides. *J. Mater. Res.* **1996**, *11* (9), 2242−2256.

(28) Fu, J.; Ren, X.; Yan, S.; Gong, Y.; Tan, Y.; Liang, K.; Du, R.; Xing, X.; Mo, G.; Chen, Z.; Cai, Q.; Sun, D.; Wu, Z. Synthesis and Structural Characterization of ZnO Doped with Co. *J. Alloys Compd.* **2013**, *558* (0), 212−221.

(29) Kang, W.; Spanjers, C. S.; Rioux, R. M.; Hoefelmeyer, J. D. Synthesis of Brookite TiO_2 Nanorods with Isolated Co(ii) Surface Sites and Photocatalytic Degradation of 5,8-Dihydroxy-1,4-Naphthoquinone Dye. *J. Mater. Chem. A* **2013**, *1* (26), 7717−7728.

(30) Bekermann, D.; Gasparotto, A.; Barreca, D.; Devi, A.; Fischer, R. A. P-Co_3O_4/n-ZnO, Obtained by PECVD, Analyzed by X-Ray Photoelectron Spectroscopy. *Surf. Sci. Spectra* **2011**, *18* (1), 36.

(31) Li, P.; Wang, S.; Li, J.; Wei, Y. Structural and Optical Properties of Co-Doped ZnO Nanocrystallites Prepared by a One-Step Solution Route. *J. Lumin.* **2012**, *132* (1), 220−225.

(32) Heiba, Z. K.; Arda, L. XRD, XPS, Optical, and Raman Investigations of Structural Changes of nanoCo-Doped ZnO. *J. Mol. Struct.* **2012**, *1022* (0), 167−171.

(33) Wang, S.; Li, P.; Liu, H.; Li, J.; Wei, Y. The Structure and Optical Properties of ZnO Nanocrystals Dependence on Co-Doping Levels. *J. Alloys Compd.* **2010**, *505* (1), 362−366.

(34) Tarwal, N. L.; Gurav, K. V.; Prem Kumar, T.; Jeong, Y. K.; Shim, H. S.; Kim, I. Y.; Kim, J. H.; Jang, J. H.; Patil, P. S. Structure, X-Ray Photoelectron Spectroscopy and Photoluminescence Investigations of the Spray Deposited Cobalt Doped ZnO Thin Films. *J. Anal. Appl. Pyrolysis* **2014**, *106* (0), 26−32.

(35) Beltrán, J. J.; Barrero, C. A.; Punnoose, A. Identifying the Sources of Ferromagnetism in Sol-Gel Synthesized $Zn_{1-x}Co_xO$ ($0 \leq x \leq 0.10$) Nanoparticles. *J. Solid State Chem.* **2016**, *240*, 30−42.

(36) Chang, J.; Ahmad, M. Z.; Wlodarski, W.; Waclawik, E. R. Self-Assembled 3D ZnO Porous Structures with Exposed Reactive {0001} Facets and Their Enhanced Gas Sensitivity. *Sensors* **2013**, *13* (7), 8445.

(37) Vijayaprasath, G.; Murugan, R.; Shankara Narayanan, J.; Dharuman, V.; Ravi, G.; Hayakawa, Y. Glucose Sensing Behavior of Cobalt Doped ZnO Nanoparticles Synthesized by Co-Precipitation Method. *J. Mater. Sci.: Mater. Electron.* **2015**, *26* (7), 4988−4996.

(38) Korotcenkov, G. Metal Oxides for Solid-State Gas Sensors: What Determines Our Choice? *Mater. Sci. Eng., B* **2007**, *139* (1), 1−23.

(39) Kim, H.-J.; Lee, J.-H. Highly Sensitive and Selective Gas Sensors Using p-Type Oxide Semiconductors: Overview. *Sens. Actuators, B* **2014**, *192*, 607−627.

(40) Woo, H.-S.; Kwak, C.-H.; Chung, J.-H.; Lee, J.-H. Co-Doped Branched ZnO Nanowires for Ultraselective and Sensitive Detection of Xylene. *ACS Appl. Mater. Interfaces* **2014**, *6* (24), 22553−22560.

(41) Zhu, G.; Xu, H.; Liu, Y.; Xu, X.; Ji, Z.; Shen, X.; Xu, Z. Enhanced Gas Sensing Performance of Co-Doped ZnO Hierarchical Microspheres to 1,2-Dichloroethane. *Sens. Actuators, B* **2012**, *166−167* (0), 36−43.

(42) Kumar, R.; Al-Dossary, O.; Kumar, G.; Umar, A. Zinc Oxide Nanostructures for NO_2 Gas–Sensor Applications: A Review. *Nano-Micro Lett.* **2015**, *7* (2), 97−120.

(43) Eranna, G.; Joshi, B. C.; Runthala, D. P.; Gupta, R. P. Oxide Materials for Development of Integrated Gas Sensors - A Comprehensive Review. *Crit. Rev. Solid State Mater. Sci.* **2004**, *29* (3−4), 111−188.

(44) Ahn, M.-W.; Park, K.-S.; Heo, J.-H.; Park, J.-G.; Kim, D.-W.; Choi, K. J.; Lee, J.-H.; Hong, S.-H. Gas Sensing Properties of Defect-Controlled ZnO-Nanowire Gas Sensor. *Appl. Phys. Lett.* **2008**, *93* (26), 263103.

(45) An, W.; Wu, X.; Zeng, X. C. Adsorption of O_2, H_2, CO, NH_3, and NO_2 on ZnO Nanotube: A Density Functional Theory Study. *J. Phys. Chem. C* **2008**, *112* (15), 5747−5755.